

Analyzing Performance of THz Band Graphene-Based MIMO Antenna for 6G Applications

Noor S. Asaad, Adham M. Saleh, and Mahmud A. Alzubaidy

Ninevah University, Mosul, Iraq

<https://doi.org/10.26636/jtit.2024.3.1518>

Abstract — In this paper, a compact 2×2 hexagon ring-shaped MIMO antenna operating at the terahertz band is proposed for future 6G wireless communication applications. The antenna is designed using graphene, due to its unique high-speed transmission capabilities. DGS and NL decoupling approaches are applied to enhance isolation between the two radiating elements. A parametric study is performed to investigate the significance of using these methods. Performance in terms of different metrics is studied using the CST Microwave Studio simulator. The final outcomes show that the proposed MIMO antenna achieves 23 dB of isolation, 0.004859 of ECC, 0.004 bits/sec/Hz of CCL, and efficiency of 98%.

Keywords — 6G, DGS, graphene, MIMO antenna, NL, THz band

1. Introduction

According to [1], [2], 6G will be the first wireless technology to transmit data at terabits per second and is intended to be launched in the future, between 2027 and 2030 [3]. For the development of 6G communication technologies, terahertz bands are advised to be used which are located between microwave and infrared ranges, and their spectrum varies from 0.1 to 10 THz [4]–[6].

It is critical to recognize that graphene, which works as conducting material in antennas, has numerous advantages at the THz band, such as high carrier mobility enabling very fast transport of charges and resulting in enhanced performance of the antenna. On the other hand, the main difference between graphene and metal conductors lies in the level of losses at the THz band. Graphene exhibits low losses at the terahertz band which, in turn, improves antenna efficiency [3]–[4].

Furthermore, graphene may be deposited onto substrates using different techniques, such as chemical vapor deposition (CVD), double self-assembly (DSA), and offers good adhesion strength. These methods open the way to develop lightweight, flexible, and efficient electronic devices [5].

Multiple-input multiple-output (MIMO) antennas are one of the most significant developments in mobile communications achieved in recent years. In this type technology, several antennas are placed at fixed locations on the transmitter and receiver, apart from one another [7]. The main benefit of using a MIMO antenna consists in the provision of high data rates and reduction of latency by transmitting data simultaneously

over several channels. Therefore, it is essential to mention here that MIMO technology at the THz band can be considered the backbone of 6G communication systems [8]–[10]. In multi-antenna technologies, the isolation between the radiating elements is affected considerably by the separation between them. Good isolation may be obtained by increasing the distance between the elements. Low envelope correlation coefficient (ECC) values, as well as high diversity gain (DG) and channel capacity loss (CCL) values may be achieved together with high isolation [4].

There are many papers aiming to improve MIMO performance at the THz band. For example, the authors in [11] designed a proximity-coupled graphene patch-based 2×2 MIMO antenna. No decoupling method was mentioned in this design to enhance performance. On the other hand, the authors of [12] presented an elliptical-shaped microstrip feed super wide band (SWB) 2×2 MIMO antenna for the terahertz band. In this design, L-shaped decoupling was added to the ground plane to improve performance.

In [13], the authors proposed a 4×4 MIMO antenna with SWB at THz frequencies. The isolation between elements was improved by applying three different fractal antenna configurations. Furthermore, paper [4] suggested a graphene MIMO patch antenna using E-shaped metamaterial unit cells to reduce coupling by placing it between the patches. Article [14] presented a 4×4 MIMO antenna for the THz band, where the decoupling between the elements was achieved by placing the elements at different orientations.

It can be clearly seen from these studies that there is a lack of investigations concerning the effect of other decoupling methods in MIMO antennas and of their impact on performance parameters. Therefore, in this paper, a graphene-based MIMO antenna operating at the THz band for 6G applications is presented. The design consists of 2×2 monopole antennas. To increase antenna performance and improve isolation between the radiating elements, defected ground structure (DGS) and neutralization line (NL) techniques are employed.

Performance characteristics of the single-element antenna and MIMO antennas are investigated to determine applicability for 6G applications. Finally, due to the difficulty of fabricating the proposed design, CST Microwave Studio (CST), High-Frequency Structure Simulator (HFSS), and Advanced Design

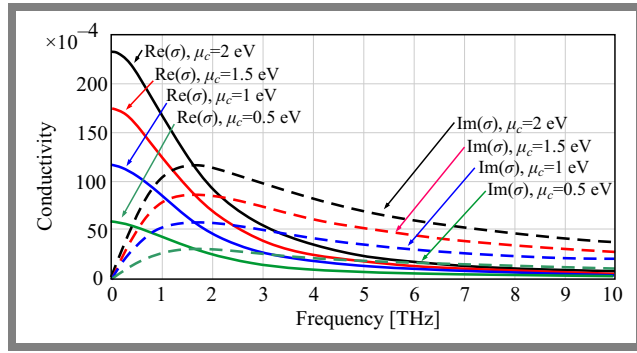


Fig. 1. Overall graphene conductivity vs. frequency for different chemical potential values.

System (ADS) software RF simulators are used to simulate the proposed solution.

2. Antenna Design

Graphene is a 2D carbon film with its thickness being equal to that of a single atomic layer [15]. In antenna applications, two aspects of its surface conductivity may be considered: intra-band, which covers the frequency range below 5 THz, and inter-band, covering frequencies above 5 THz [13]. The parameters of graphene in these two categories depend on chemical potential, frequency of operation, temperature and relaxation time, as shown by the following equations [6]:

$$\sigma_{intra} = -j \frac{e^2 k_B T}{\pi h^2 (\omega - j\tau^{-1})} \left[\frac{\mu c}{k_B T} + 2 \ln(e^{-\frac{\mu c}{k_B T}} + 1) \right], \quad (1)$$

$$\sigma_{inter} = \frac{j e^2}{4\pi h} \ln \frac{2|\mu c| - h(\omega - j\tau^{-1})}{2|\mu c| + h(\omega - j\tau^{-1})}, \quad (2)$$

where T represents temperature, h represents reduced Planck's constant, k_B is Boltzmann constant, μc stands for chemical potential in eV, e is electron charge, τ represents the relaxation time and its value is 0.1 ps at room temperature, and, finally, ω is the frequency of operation.

The total intra-band and inter-band surface conductivity may be calculated as:

$$\sigma_s = \sigma_{inter} + \sigma_{intra}. \quad (3)$$

The overall conductivity of the graphene layer is shown in Fig. 1 with different chemical potentials. It is clearly seen that changing the chemical potential has a high impact on overall surface conductivity. On the other side, the chemical potential affects the carrier density by applying an external gate voltage [6]. This property can be very helpful in controlling the resonant frequency in antenna design processes.

3. Simulation Results

3.1. Single Antenna Design

The proposed shape with one radiating element is shown in Fig. 2. It consists of a hexagon ring that uses teflon with

a dielectric constant ϵ_r of 2.1 and thickness h of 10 μm . The hexagon ring is printed above the dielectric surface while the ground plane is located underneath it. The overall dimensions of the presented element are $53 \times 35 \times 10 \mu\text{m}^3$. Graphene is used as a conducting material due to its unique features, such as reducing antenna losses and high-speed conductivity within the THz band. The thickness of graphene is set at 35 nm. The antenna is also fed by a microstrip line with a size of $15.13 \times 3.60 \mu\text{m}^2$.

The final dimensions of the proposed structure are listed in Tab. 1. The simulation target is determined to design an antenna that covers the terahertz band with a resonant frequency of approximately 3 THz. The design is simulated with different values of the applied chemical potential (from 0 to 2 eV) to achieve the resonant frequency. The simulated reflection coefficient is illustrated in Fig. 3. It can be clearly noted that the operating frequency is affected by changing the chemical potential and varies from 2.62 to 3.67 THz with $S_{11} \leq -10$ dB by applying $\mu_c = 2$ eV.

After that, the equivalent circuit of the proposed antenna is simulated by the ADS software to enhance the results obtained from CST and HFSS, as shown in Fig. 4. A comparison between the simulated S_{11} obtained from the three different

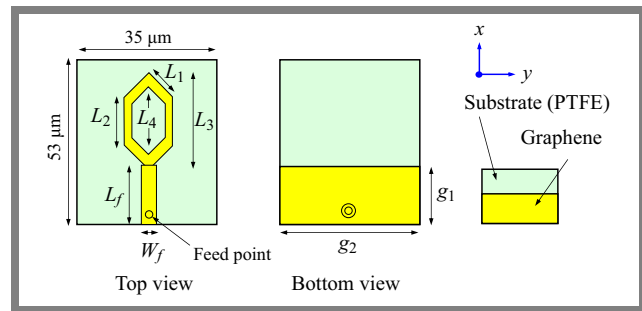


Fig. 2. Details of the hexagon ring antenna design.

Tab. 1. Dimensions of one radiating element in [μm].

| Parameter | L_1 | L_2 | L_3 | L_4 |
|-----------|-------|-------|-------|-------|
| Value | 8.50 | 12.02 | 24.04 | 16.83 |
| Parameter | g_1 | g_2 | w_f | L_f |
| Value | 14.70 | 35 | 3.60 | 15.13 |

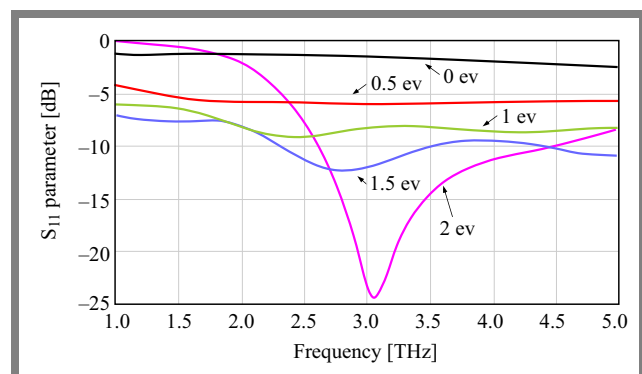


Fig. 3. Simulated result of S_{11} for a single hexagon ring antenna for different chemical potential values.

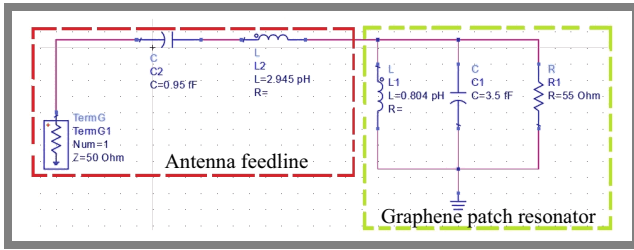


Fig. 4. Equivalent circuit model for the proposed single antenna.

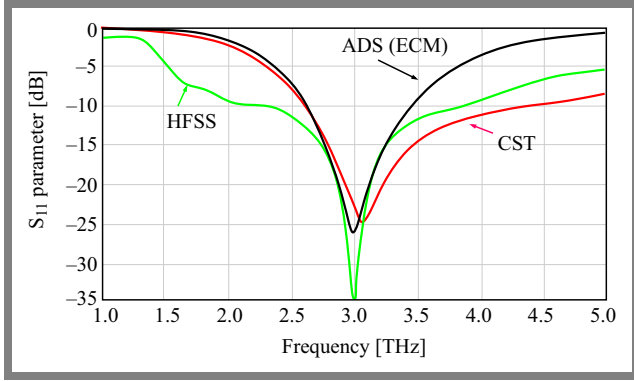


Fig. 5. Simulated S_{11} for the single element antenna with CST, HFSS, and ADS equivalent circuit.

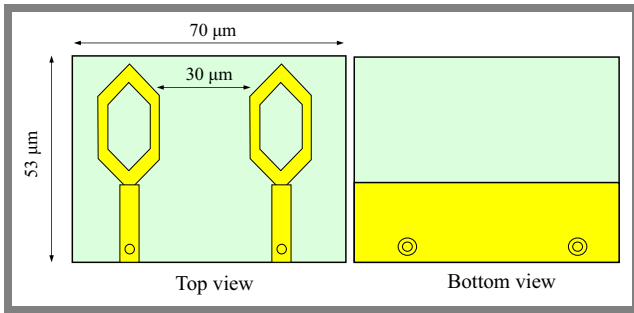


Fig. 6. Dimensions of the proposed 2x2 MIMO antenna.

simulators is illustrated in Fig. 5. As one may notice, the figure shows a perfect agreement between the obtained results.

3.2. Two-Element MIMO Antenna Design

In this part, a 2x2 MIMO hexagon ring antenna is designed as a single structure, as shown in Fig. 6. The distance between the two antenna elements is 30 μm and the dimensions of the ground plane equal 70x14.70x0.035 μm³. The total size of the presented antenna is 53x70x10 μm³.

The equivalent circuit of the proposed two-element MIMO antenna from the ADS simulator is presented in Fig. 7. Figure 8 shows the simulated S_{11} of the 2x2 MIMO antenna from the three different simulation software instances. It is clear from CST results that the antenna works from 2.47 to 3.44 THz, with a resonant frequency of 2.8 THz. It has been also observed that the resonant frequency has been shifted to a lower value compared to the single antenna case. This stems from mutual coupling between the two radiating elements.

The simulated transmission coefficient S_{21} is shown in Fig. 8. This plot proves that mutual coupling S_{21} between the two radiating elements is less than -15 dB for the 2.02 to 2.5 THz

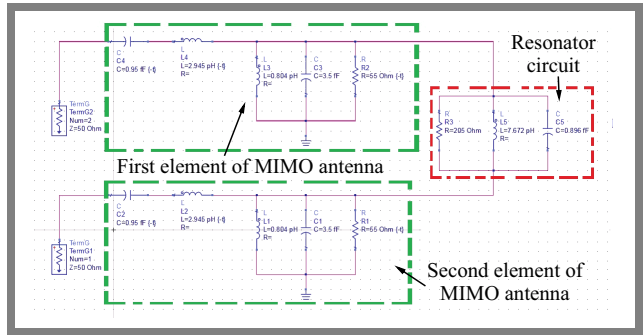


Fig. 7. Equivalent circuit model of the proposed 2x2 MIMO configuration.

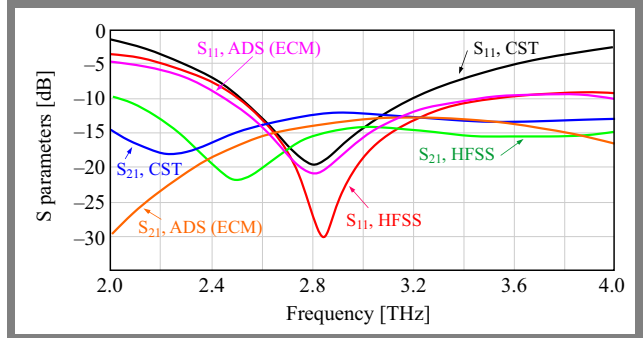


Fig. 8. S parameter values for a 2x2 MIMO antenna simulated with CST, HFSS, and ADS software.

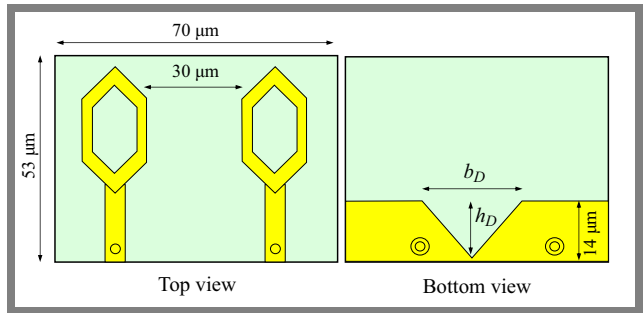


Fig. 9. Proposed geometry of a 2x2 MIMO hexagon ring antenna with DGS.

range. As the frequency ranges for S_{11} and S_{21} are not the same, mutual coupling should be reduced below -15 dB for the entire operating range. Finally, a good agreement between the results of CST, HFSS and ADS is achieved.

3.3. MIMO Antenna with DGS Decoupling Approach

Defected ground structure (DGS) is an etched-out area on the ground plane of a microstrip PCB. It is a beneficial method that is used to improve the gain and the bandwidth of printed antennas. It can be also used to reduce coupling between radiating elements in multi-antenna technologies, due to its unique feature of inserting virtual inductances and capacitances into the structure of the MIMO antenna. Hence, it may act as a stop band filter. A defective area on the ground plane is represented by a triangular shape in the middle between the two elements, as shown in Fig. 9.

The effects of height h_D and base b_D of the defective area are studied to achieve the lowest results in terms of mutual

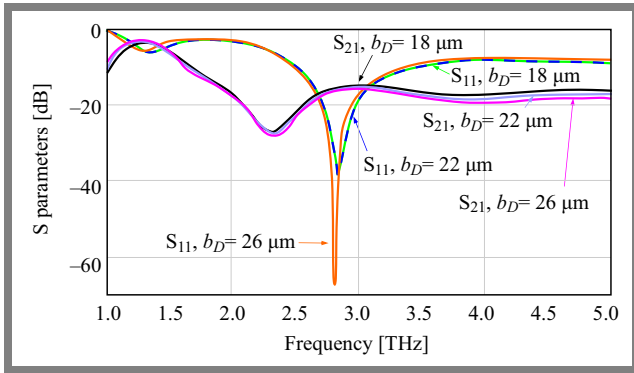


Fig. 10. Simulated S_{11} and S_{21} for a 2×2 MIMO hexagon ring antenna with DGS: $h_D = 14 \mu\text{m}$ and variable b_D .

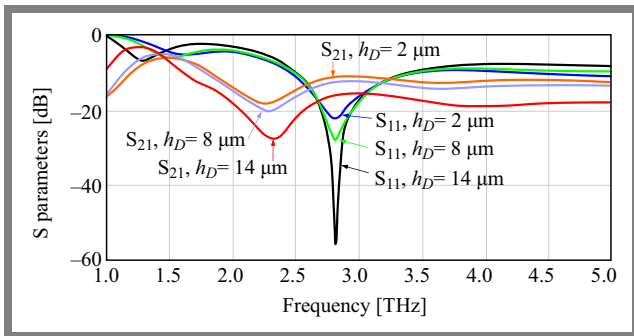


Fig. 11. Simulation of S_{11} and S_{21} for a 2×2 MIMO hexagon ring antenna with DGS: $b_D = 26 \mu\text{m}$ and variable h_D .

coupling. The analysis starts by setting height h_D to the maximum value of $14 \mu\text{m}$ and changing the length of base b_D . The initial value of b_D is fixed at $18 \mu\text{m}$ and then different lengths of b_D are tested.

Figure 10 illustrates the reflection and transmission coefficients obtained for different values of b_D . One may notice that the frequency band of the reflection coefficient S_{11} is slightly affected by changing the length of b_D and the magnitude of S_{11} is reduced significantly by increasing b_D . The best value is obtained at $b_D = 26 \mu\text{m}$ with $|S_{11}|$ equaling -67 dB .

On the other hand, isolation is improved by increasing the length of b_D and the antenna achieved an isolation value of more than 15 dB for the entire frequency band. Another study concerning the parameters of the defected area consists in assuming a constant value of the base ($b_D = 26 \mu\text{m}$) and changing height h_D . Three different h_D values are tested and the outcomes of the simulated reflection and transmission coefficients are presented in Fig. 11.

The same dependence as described in the first parametric study is noticed in this case as well, i.e. an increase in h_D leads to a reduction in the magnitude of S_{11} and in enhancing the isolation between the two antennas. From this simulation, we can conclude that the optimum dimensions for the defected area equal $h_D = 14 \mu\text{m}$ and $b_D = 26 \mu\text{m}$.

3.4. MIMO Antenna with Three DGSs

This section investigated the use of the DGS technique in a MIMO antenna, in three different regions. The first cut has a triangular shape and is located in the middle between the

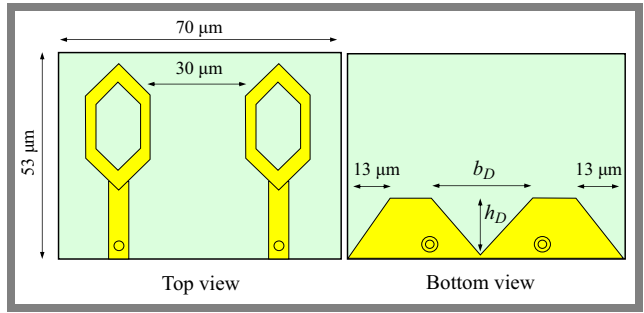


Fig. 12. A 2×2 MIMO hexagon ring antenna with three DGS.

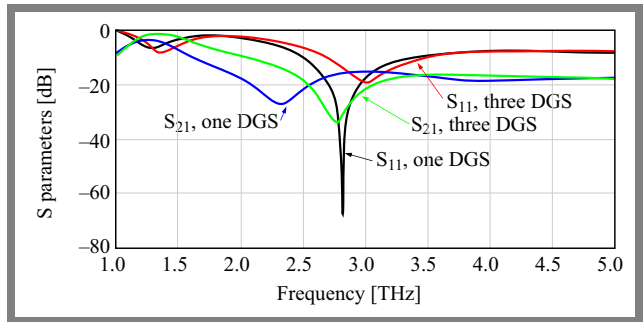


Fig. 13. Simulated results of S_{11} and S_{21} for a 2×2 MIMO hexagon ring antenna with one and three DGSs.

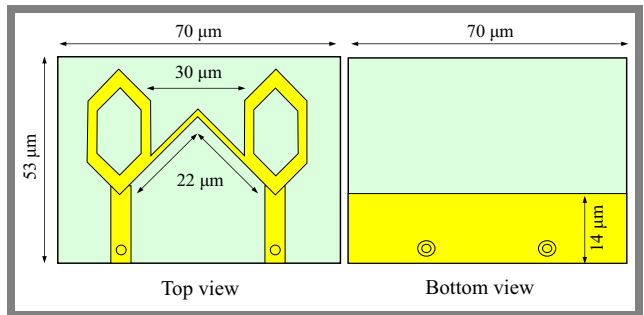


Fig. 14. A 2×2 MIMO hexagon ring antenna with NL.

two radiating elements with dimensions $b_D = 26 \mu\text{m}$ and $h_D = 14 \mu\text{m}$. The second and third DGSs have the shape of a half triangle, as shown in Fig. 12.

The comparison between the simulated results of S_{11} and S_{21} and the three DGSs are shown in Fig. 13. By applying the three DGSs, the resonant frequency of the reflected coefficient is shifted to the upper band and the achieved bandwidth is widened slightly. The mutual coupling band is also shifted to the upper band and the antenna achieves a lower mutual coupling value within the operating frequency band, i.e. 22 dB at the resonant frequency, compared to -17 dB for a solution with one DGS.

3.5. MIMO Antenna Design Based on NL Decoupling Approach

Coupling in MIMO antennas may be reduced by adding a neutralization line between the radiating elements. In this technique, the current in one position is neutralized by using a sample with an inverted phase, so it can cancel the current from the other radiating element.

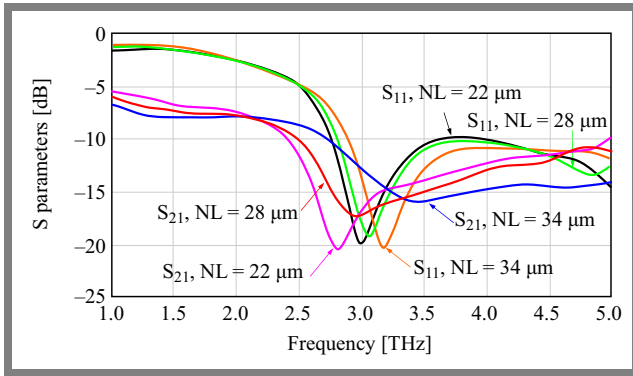


Fig. 15. Simulated outcomes of S_{11} and S_{21} for a 2×2 MIMO hexagon ring antenna with NL.

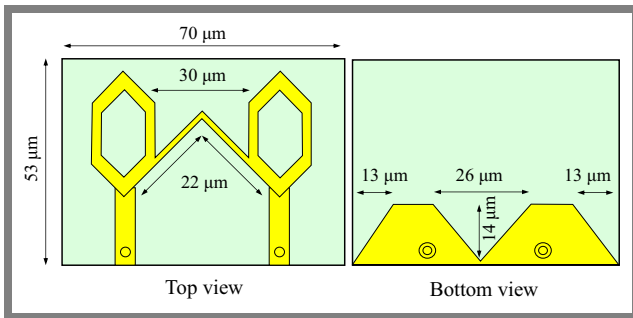


Fig. 16. A 2×2 MIMO hexagon ring antenna with NL and with DGS.

The technique is incorporated by using NL in the form of a triangle with a total length of $22 \mu\text{m}$, as shown in Fig. 14. During simulation, the length of NL was varied to achieve the optimum (lowest) coupling value. S_{11} and S_{21} results are illustrated in Fig. 15. It may be noted that two different phenomena appeared by adding NL. The first one consists in the fact that the resonant frequency is shifted toward the upper frequency band, while the other is that a decrease in the length of NL leads to shifting the resonant frequency towards the lower frequency band. Coupling between the elements is reduced with a longer neutralization line. Isolation of more than 15 dB is obtained around the resonant frequency with NL of $22 \mu\text{m}$.

To further analyze the obtained results, the dependence between the length of NL and the wavelength inside the substrate λ_d is simulated by determining the ratio between these values. The following equations are used to calculate λ_d inside the substrate:

$$\epsilon_{eff} = \frac{\epsilon_r + 1}{2}, \quad (4)$$

$$\lambda_d = \frac{\lambda_o}{\sqrt{\epsilon_{eff}}}, \quad (5)$$

where λ_o represents wavelength in free space, λ_d is wavelength inside the substrate, ϵ_{eff} stands for effective permittivity and ϵ_r represents relative permittivity.

The obtained NL-to- λ_d ratio is 98% at 2.8 THz, at the resonant frequency without using any decoupling methods. This ratio proves high correlation and shows that NL is working properly.

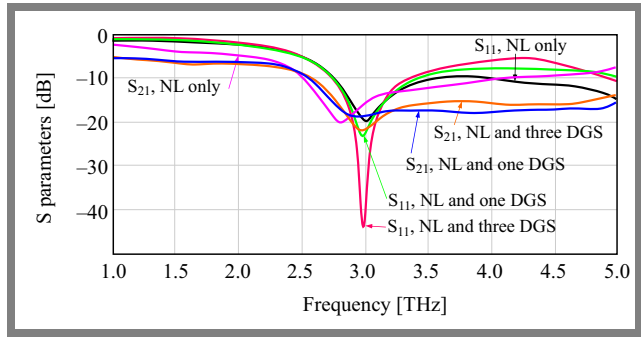


Fig. 17. Simulated results of S_{11} and S_{21} for a 2×2 MIMO hexagon ring antenna with NL for three different cases.

3.6. MIMO Antenna with DGSs and NL Decoupling Methods

Finally, the proposed design of a 2×2 MIMO hexagon ring antenna was tested by combining the NL decoupling method with DGS, as shown in Fig. 16. The simulated values of reflection coefficient S_{11} and transmission coefficient S_{21} are compared, as shown in Fig. 17.

The resonant frequency is 3 THz in all simulations and the magnitude is significantly reduced, reaching -45 dB for the scenario with NL and three DGSs. Coupling is also reduced at the resonant frequency and reaches -23 dB at 3 THz.

4. Performance Evaluation

To assess the performance of the proposed design, a range of parameters, such as channel capacity loss (CCL), total active reflection coefficient (TARC), diversity gain (DG) and envelope correlation coefficient (ECC) is determined. ECC-related results for all six cases are presented in Fig. 18a – in all of the scenarios ECC is below 0.1 at the resonant frequency. DG values (Fig. 18b) simulated for all the cases equal approximately 10 dB at the resonant frequency, while CCL (Fig. 18c) is approximately zero at the resonant frequency which is below 0.4 bit/s/Hz, i.e. reaches the limit for a MIMO antenna. Finally, TARC is determined (Fig. 18d) for different phase angles at 30° steps, covering the range from 0 to 180° . TARC is below 6 dB at the resonant frequency and in drops, in some cases, below 10 dB.

Simulations of the proposed antenna's total efficiency for all three cases are summarized in Fig. 19a. The highest efficiency of 98% is achieved in the case of NL and DGSs, compared with all other cases at the operating frequency of 3 THz.

The realized gain (Fig. 19b) at the resonant frequency is approximately 2 dB for all the cases. Finally, far field radiation patterns are plotted in 3D for the case of NL and DGSs in Fig. 20, showing the antenna's omnidirectional pattern.

Table 2 summarizes the parameters of similar antennas from the literature and compares them with the proposed design. It is clear from this comparison that the proposed design is characterized by the smallest physical size. This can be very helpful in increasing the number of radiating elements when adopting massive MIMO.

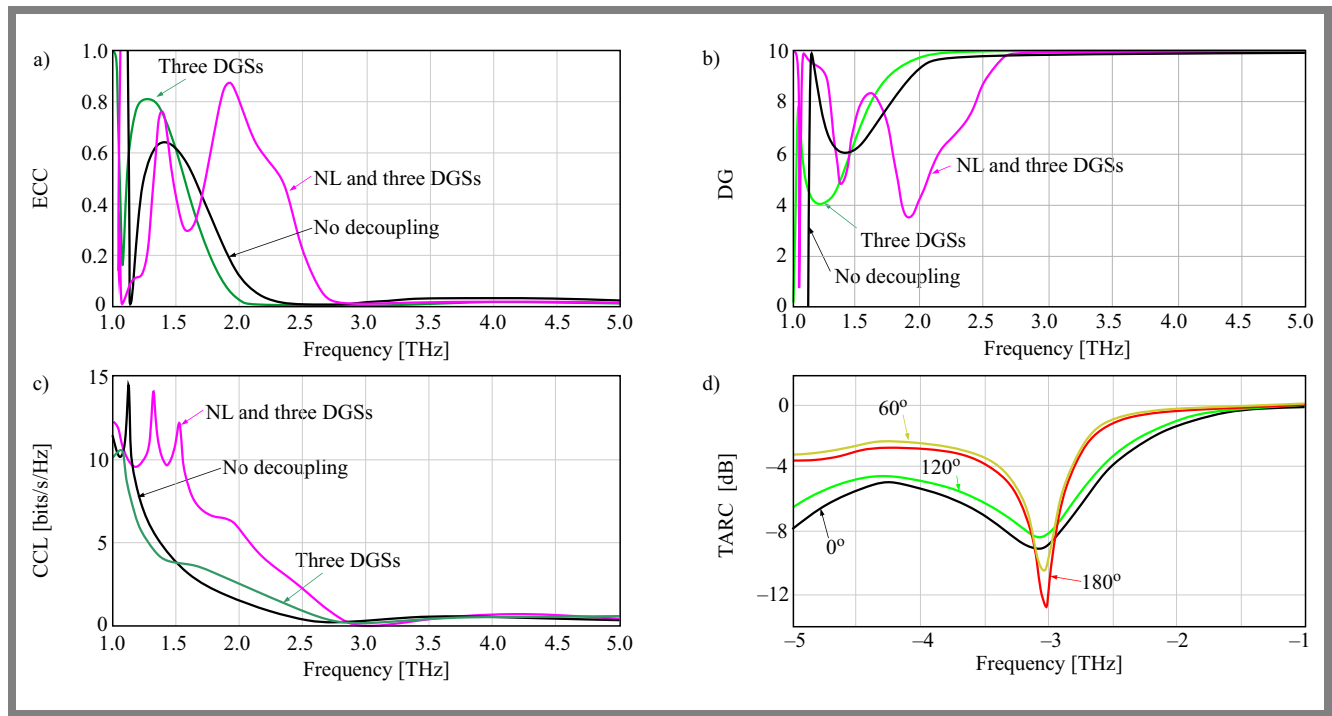


Fig. 18. Simulations of: a) ECC, b) DG, c) CCL, and d) TARC of the proposed antenna.

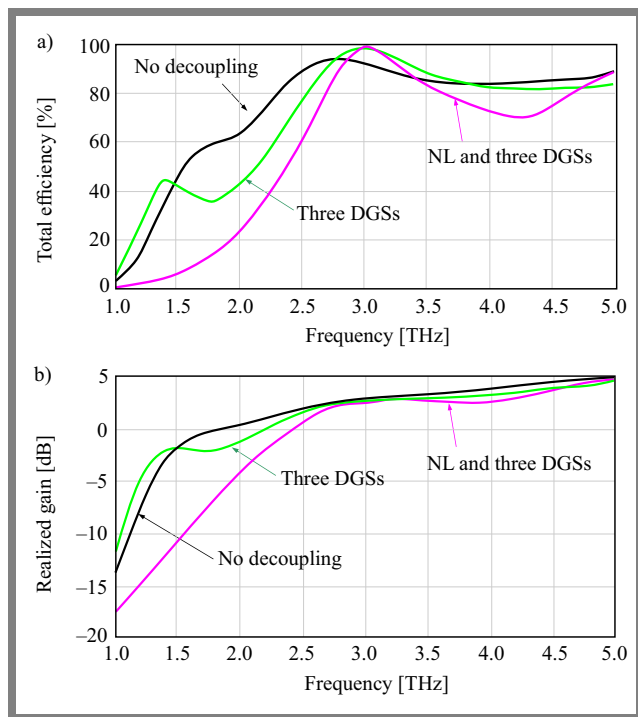


Fig. 19. Total efficiency a) and realized gain b).

On the other hand, the antenna achieves high efficiency compared with other works. Furthermore, the coupling of the design is below -15 dB for the entire band and -23 dB at the resonant frequency. This means that only 0.5% of the applied power will be coupled to the adjusting antenna at the resonant frequency.

This comparison reveals that this MIMO antenna offers promising performance in the terahertz band.

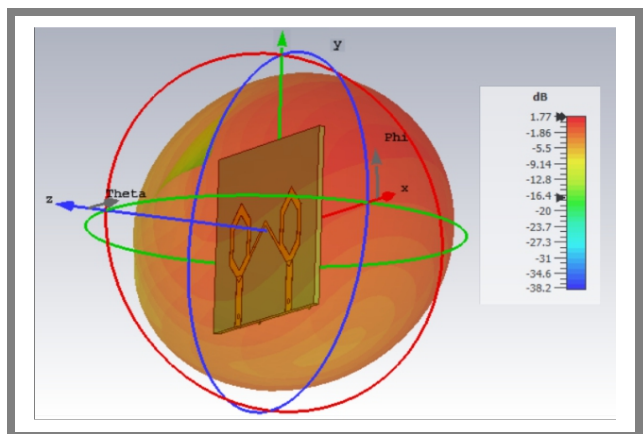


Fig. 20. Simulated 3D radiation pattern for the case with NL and DGSs.

5. Conclusion

This paper presents a two-element compact MIMO antenna utilizing graphene, intended for operating in the THz band for use in upcoming 6G applications. Mutual coupling inside the antenna structure has been minimized by applying two different decoupling approaches. It has been noticed the best isolation value is achieved when the two design approaches are combined together. The value obtained for the combined decoupling approach is -23 dB at the resonant frequency of 2.8 THz. The fundamental characteristics of the proposed MIMO antenna have been studied in terms of ECC, DG, TARC, CCL, antenna gain, efficiency, and antenna radiation pattern. The outcomes show that the antenna may serve as a good candidate for deployment in future 6G applications.

Tab. 2. Comparison with other works.

| Ref. | Resonant frequency [THz] | Antenna size [μm^2] | Mutual coupling [dB] | CCL [bits/sec/Hz] | Antenna efficiency | DG [dB] | ECC |
|-----------|--------------------------|----------------------------------|----------------------|-------------------|--------------------|---------|----------|
| [4] | 1.9 | 120×90 | -54 | 0.0014 | - | 9.99 | 0.000023 |
| [11] | 1.82 | 60×40 | -25 | - | 80% | 9.95 | - |
| [12] | 0.33–10 | 1000×1400 | -25 | 0.25 | 70% | 9.99 | 0.0015 |
| [13] | 1.42 | 125×125 | -20 | 0.31 | - | 9.98 | 0.0022 |
| [14] | 7.1–13 | 100×100 | -18 | - | - | 9.97 | 0–0.5 |
| This work | 2.8 | 70×35 | -23 | 0.004 | 98% | 9.99 | 0.004859 |

References

- [1] S. Elmeadawy and R.M. Shubair, “Enabling Technologies for 6G Future Wireless Communications: Opportunities and Challenges”, 2020 (<https://doi.org/10.48550/arXiv.2002.06068>).
- [2] F. Tariq *et al.*, “A Speculative Study on 6G”, *IEEE Wireless Communications*, vol. 27, no. 4, pp. 118–125, 2019 (<https://doi.org/10.1109/MWC.001.1900488>).
- [3] M.S. Swetha, M.S. Muneshwara, A.S.M. Hegde, and Z. Lu, “6G Wireless Communication Systems and Its Applications”, in: *Machine Learning and Mechanics Based Soft Computing Applications. Studies in Computational Intelligence*, vol. 1068, pp. 271–288, 2023 (https://doi.org/10.1007/978-981-19-6450-3_25).
- [4] S.A. Khaleel, E.K.I. Hamad, N.O. Parchin, and M.B. Saleh, “Programmable Beam-steering Capabilities Based on Graphene Plasmonic THz MIMO Antenna via Reconfigurable Intelligent Surfaces (RIS) for IoT Applications”, *Electronics*, vol. 12, no. 1, 2023 (<https://doi.org/10.3390/electronics12010164>).
- [5] A.B. Suriani *et al.*, “Synthesis, Transfer and Application of Graphene as a Transparent Conductive Film: a Review”, *Bulletin of Materials Science*, vol. 43, art. no. 310, pp. 1–14, 2020 (<https://doi.org/10.1007/s12034-020-02270-9>).
- [6] S.A. Khaleel, E.K.I. Hamad, N.O. Parchin, and M.B. Saleh, “MTM-Inspired Graphene-based THz MIMO Antenna Configurations Using Characteristic Mode Analysis for 6G/IoT Applications”, *Electronics*, vol. 11, no. 14, 2022 (<https://doi.org/10.3390/electronic11142152>).
- [7] M.H. Reddy and D. Sheela, “MIMO Antenna Design and Optimization with Enhanced Bandwidth for Wireless Applications”, *Journal of Telecommunication and Information Technology*, no. 4, pp. 22–26, 2020 (<https://doi.org/10.26636/jtit.2020.145520>).
- [8] B.-Y. Duan, “Evolution and Innovation of Antenna Systems for Beyond 5G and 6G”, *Frontiers of Information Technology and Electronic Engineering*, vol. 21, no. 1, 2020 (<https://doi.org/10.1631/FITEE.2010000>).
- [9] T.O. Olwal, P.N. Chuku, and A.A. Lysko, “Antenna Research Directions for 6G a Brief Overview Through Sampling Literature”, *7th International Conference on Advanced Computing and Communication Systems (ICACCS)*, Coimbatore, India, 2021 (<https://doi.org/10.1109/ICACCS51430.2021.9441781>).
- [10] K.K. Wong, K.F. Tong, Y. Zhang, and Z. Zheng, “Fluid Antenna System for 6G: When Bruce Lee Inspires Wireless Communications”, *Electronics Letters*, vol. 56, no. 24, pp. 1288–1290, 2020 (<https://doi.org/10.1049/el.2020.2788>).
- [11] G. Varshney, S. Gotra, V.S. Pandey, and R.S. Yaduvanshi, “Proximity-coupled Two-port Multi-input-multi-output Graphene Antenna with Pattern Diversity for THz Applications”, *Nano Communication Networks*, vol. 21, art. no. 100246, 2019 (<https://doi.org/10.1016/j.nancom.2019.05.003>).
- [12] G. Saxena, Y.K. Awasthi, and P. Jain, “High Isolation and High Gain Super-wideband (0.33-10 THz) MIMO Antenna for THz Applications”, *Optik*, vol. 223, art. no. 165335, 2020 (<https://doi.org/10.1016/j.ijleo.2020.165335>).
- [13] S. Das, D. Mitra, and S.R.B. Chaudhuri, “Fractal Loaded Planar Super Wide Band Four-element MIMO Antenna for THz Applications”, *Nano Communication Networks*, vol. 30, art. no. 100374, 2021 (<https://doi.org/10.1016/j.nancom.2021.100374>).
- [14] R.H. Abd and H.A. Abdulnabi, “Design of Graphene-based Multi-input Multi-output Antenna for 6G/IoT Applications”, *Indonesian Journal of Electrical Engineering and Computer Science*, vol. 31, no. 1, pp. 212–221, 2023 (<https://doi.org/10.11591/ijeecs.v31.i1.pp212-221>).
- [15] G.W. Hanson, A.B. Yakovlev, and A. Mafi, “Excitation of Discrete and Continuous Spectrum for a Surface Conductivity Model of Graphene”, *Journal of Applied Physics*, vol. 110, no. 11, 2011 (<https://doi.org/10.1063/1.3662883>).

Noor S. Asaad, M.Sc.

Department of Communication Engineering

 <https://orcid.org/0000-0000-0000-0000>

E-mail: noor.sabah2021@stu.uoninevah.edu.iq

Ninevah University, Mosul, Iraq

<https://uoninevah.edu.iq/en>

Adham M. Saleh, Ph.D.


 <https://orcid.org/0000-0003-4589-7491>

E-mail: adham.saleh@uoninevah.edu.iq

Ninevah University, Mosul, Iraq

<https://uoninevah.edu.iq/en>

Mahmod A. Alzubaidy, Assistant Professor

 <https://orcid.org/0000-0003-4115-9491>

E-mail: mahmod.mahmod@uoninevah.edu.iq

Ninevah University, Mosul, Iraq

<https://uoninevah.edu.iq/en>